Physics, Astronomy and Geophysics Honors Papers   Physics, Astronomy and Geophysics Department

Spring 4-30-2008

Determining the Temperature of Exoplanet HAT-P-1b

Kamen O. Todorov

Connecticut College, kamen.todorov@conncoll.edu

Follow this and additional works at: http://digitalcommons.conncoll.edu/physicshp

Part of the Astrophysics and Astronomy Commons

Determining the Temperature of Exoplanet HAT-P-1b

An Honors Thesis

Presented by

Kamen Todorov, Class of 2008

to

The Department of Physics, Astronomy and Geophysics

In partial fulfillment of the requirements for Honors in the Major Field

Co-advisors: **Dr. Drake Deming**, Planetary Systems Laboratory, NASA Goddard Space Flight Center

Dr. Leslie Brown, Department of Physics, Astronomy and Geophysics, Connecticut College

Connecticut College, New London, Connecticut

April 30, 2008

Abstract

Exoplanets, or planets orbiting stars other than our Sun, are difficult to detect. It is even more difficult to determine their properties. In this thesis I focus on HAT-P-1b, which is a "hot Jupiter" – a gas giant, extremely close to its parent star. It is important for this thesis that HAT-P-1b is also a transiting exoplanet, i.e., it periodically passes directly in front of, or behind, its parent star, which gives scientists unique opportunities to determine its physical properties, to measure its temperature and to study its atmosphere's chemical properties.

The purpose of this thesis is to measure the brightness temperature of the transiting exoplanet HAT-P-1b. The observations used were made with the Spitzer Space Telescope through a filter with center wavelength of 8.0μm, which covered a secondary eclipse of the planetary system, i.e., when the planet is behind its parent star, ADS 16402B. We created a light curve for the system, detected the eclipse and fitted a model eclipse curve in the data. From the eclipse depth I determined HAT-P-1b's flux. Knowing the planet's distance from ADS 16402B and the masses and radii of the star and the planet, I estimated the brightness temperature of the planet. My calculated result is 1300±170K. Future research will involve similar measurements in three additional wavebands, which will provide information about the chemical and thermal structure of HAT-P-1b's atmosphere.

Acknowledgements

Professor Brown, thank you for all your support and friendship through the years of college, and especially the last one. Your advice was invaluable and I will always remember what you taught me! You showed me how cool astronomy is. Thank you!

Dr. Deming, you gave me a chance to study exoplanets, and advised me through this thesis. Without your help I would have never done the most interesting project in my college career. Thank you!

Professors Mantz and Monce, I really appreciate that you taught me physics, but you taught me more than that – in your classes I learned how to think like a scientist. Professor Monce, thank you for the error bars!

Professor Weinstein, thank you for being a great teacher. If it wasn't for you and Professor Brown, I wouldn't know that teaching is so much fun. Thank you!

Thank you to all my friends who tolerated my self-isolation while writing this thesis.

To my family and to Athena, with appreciation

Table of Contents

List of Figures and Tables

Chapter 1: Introduction

Section 1.1: Introduction to Exoplanets

Exoplanets, or extrasolar planets, is a term referring to all planets that orbit stars other than our own Sun. Most exoplanets so far have been discovered by a method called Doppler spectroscopy, although there are other ways to detect extrasolar planets, which can often be more fruitful. Exoplanets are fundamentally interesting to astronomers since they provide them with deeper insight on issues such as understanding planetary system formation and behavior with time, the likelihood of planets with sizes comparable to Earth's, and the likelihood of planets on which liquid water exists. The discovered-so-far exoplanets have varying orbital periods, but tend to have sizes comparable to that of Jupiter. This study is interested in a common class of large and massive exoplanets with periods on the order of a couple of days that are very close to their suns, in other words, conditions very different from Earth's. Such planets are often called "hot Jupiters" due to their size and expected (because of their proximity to the star) high temperature. It is thought that the relatively high frequency of occurrence of "hot Jupiters"[1] may be due to bias in the detection techniques that are in use nowadays. Planets with Earth-like conditions are deemed extremely important, because of their potential for life, but so far only one planet has been discovered that is Earth-sized and at the right distance from the star to ensure the possibility of liquid water (Udry et al. 2007).

The first discovery of exoplanets in the early 1990s has significantly changed our perspective on the Solar System. The first two extrasolar planets were discovered in 1992

---

[1] 72 out of 277 (Schneider 2008)

in orbit around a neutron star – the pulsar B1257+12 (Wolszczan 1994). Such a harsh parent star cannot possibly have planets hosting life as we know it. The first exoplanet orbiting a main sequence star, 51 Pegasi b, was discovered in 1995 by M. Mayor and D. Queloz (Mayor and Queloz 1995). Since then, up to this day, at least 277 planets have been found orbiting around stars other than the Sun (Schneider 2008) and the study of extrasolar planets is a rapidly growing area of research.

Section 1.2: Several Methods of Discovery and Observation of Exoplanets

There are a number of ways to detect an extrasolar planet, the most important of which are described below. But first, if we want to discover or to study a stellar system containing an exoplanet, we need to consider the relative position of the system and the Earth. We can define an angle, i, to be the inclination angle of the planetary system to the plane of the sky from Earth's point of view (see Figure 1.1).

Now, we can define the proper motion of the star to be the component of the star's velocity parallel to the plane of the sky, and the radial velocity of the star to be the component of its velocity perpendicular to the plane of the sky. Let us also define a coordinate system – let the x-axis be parallel to the semimajor axis of the orbit, the y-axis be parallel to the semiminor axis of the orbit and the z-axis be perpendicular to the plane of the orbit.

The most common detection method is called Doppler spectroscopy. It relies on the fact that the star and the planet are orbiting around a common center of gravity, close to, but not coinciding with, the center of the star. The orbit of the star around the common center of gravity of the system is seen from Earth as periodic changes in the star's radial
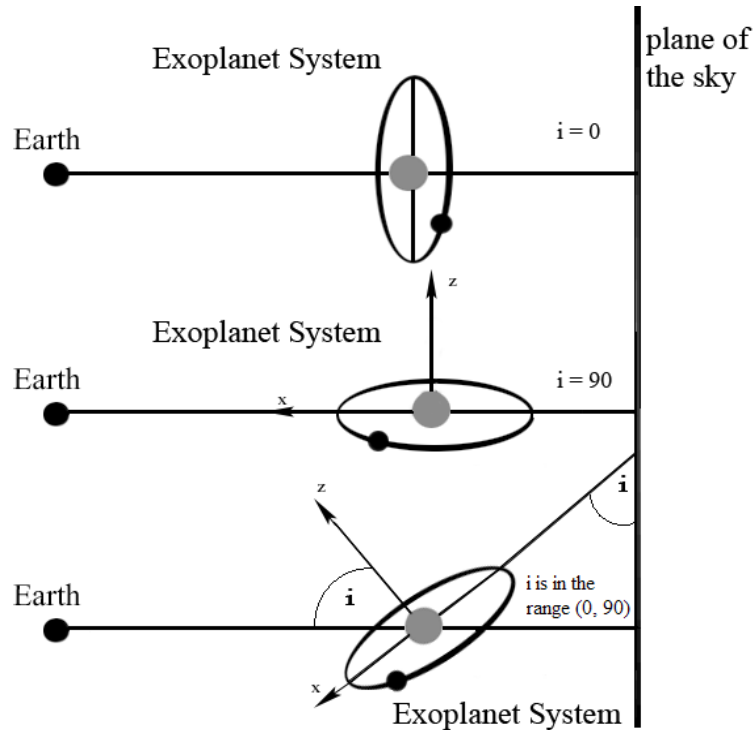
Figure 1.1: *The inclination angle, i, is defined as the angle between the plane of the exoplanet's orbit and the plane of the sky* (Zeilik and Gregory 1998, 236).

velocity – as it moves along its orbit, sometimes the star is going away from Earth and sometimes it is moving towards Earth. The periodic shifts of the star's location (which we cannot observe directly) and the periodic changes in its radial velocity (which we can detect) caused by the gravitational pull from an unseen companion are often referred to as "wobble." If the angle *i* is larger than 0°, i.e., the orbital plane of the planet is not parallel to the plane of the sky, we can see a periodic change in the radial velocity of the star; this is detected by Doppler shift measurements[1]. From these observations we can find the period of the planet's orbit, which is equal to the period of the star's orbit around the common center of gravity and hence to the period of the Doppler shifts. If we know the

---

[1] Note that if the plane of the system is parallel to plane of the sky from Earth's point of view, i.e. *i* = 0°, then we would only "see" a change in the proper motion of the star (if the system was close enough and the planet massive enough to induce angular changes in the position of the star sufficiently large to be observable from Earth). There will be no Doppler shifts at all in this case, so we would not see any evidence for a planet in the spectrum of such a system.

star's spectral class we can obtain an estimate of the star's mass, and then we can draw conclusions about the planet's semimajor axis using Newton's revision of Kepler's Third Law (Butler et al. 2006):

$$P^2 = \frac{4\pi^2 a_p^3}{G(M_* + m_p)} \ .$$
[1.1]

Here, P is the period of rotation in seconds, M_* is the mass of the star in kilograms, m_p is the mass of the planet in kilograms, a_p is the semimajor axis of the planet in meters and G is the universal constant of gravity in meters cubed per kilogram per second squared. For simplicity we assume that the eccentricity of the planet's orbit is essentially zero. It is also reasonable to assume that $M_* \gg m_p$, so that $M_* \approx M_* + m_p$. Then, we can solve for a_p to get an estimate of the semimajor axis of the planet's orbit:

$$a_p = \left[\frac{P^2 G M_*}{4\pi^2} \right]^{1/3} \ .$$
[1.2]

This is done assuming that the center of the star is the center of gravity of the system; however, this is a reasonable approximation for our purposes, since if $M_* \gg m_p$, then a_p will be much bigger than the star's semimajor axis, a_*, so we can neglect a_* for the moment. We can now make an estimate of the semimajor axis of the star's orbit around the common center of gravity. Here we assume that the inclination angle, *i*, is 90°, and that the semimajor axis of the orbit points toward Earth. This makes the radial velocity (which is a function of time), $V_r(t)$, equivalent to $V_x(t)$, the component of the orbital velocity along the x-axis of the orbit, if we define the semimajor axis of the star's orbit to be the x-axis of our coordinate system. We also assume that the motion of the star-planet system through space has been removed from the star's radial velocity. We can only

observe the radial component of the star's velocity (the planet is too faint), and we can ignore the star's proper motion component of its total velocity. Additionally, it takes ½ of the period for the star to come from the farthest position in its orbit with respect to Earth to its closest position (i.e. radial distance of twice its semimajor axis), and therefore it needs ¼ of the period to cover a radial distance equivalent to its semimajor axis. Then,

$$a_* = \int_0^{\frac{P}{4}} V_x dt \,, \qquad [1.3]$$

where dt is the change in time in seconds, a_* is the semimajor axis of the star in meters, and V_x is equal to the radial velocity of the star in meters per second, which we get from measurements of the Doppler shifts. This is just an approximation, but it holds as long as the eccentricity of the star's orbit is not large, so that the major axis is not much bigger than any other axis. We can now use the following equation to solve for the mass of the planet (Carroll and Ostlie 1996):

$$\frac{M_* a_* - m_p a_p}{M_* + m_p} = 0 \,. \qquad [1.4]$$

Or, after we solve for m_p,

$$m_p = \frac{M_* a_*}{a_p} \,. \qquad [1.5]$$

Notice, that this is only a minimum limit for the mass of the planet, because we assumed that the orbital plane is perpendicular to the sky. If it is not, then we can correct the velocity V_x by dividing V_r by $\sin(i)$, if i is known:

$$V_x = \frac{V_r}{\sin(i)} \,. \qquad [1.6]$$

This correction can make V_x significantly bigger and thus make the semimajor axis of the star in Equation [1.3] much larger. A bigger value for a_* in turn results in a larger value for m_p. Therefore, we cannot normally put an upper limit to the mass using the Doppler shift method, since, we usually do not have a way to determine i.

Although Doppler spectroscopy is the most often used method, and most planets are discovered using it, all the information it normally supplies is the semimajor axis of the planet, its period and a lower limit on the planet's mass. Also, since it is easier to detect stars with large V_x, and therefore small a_p and large m_p, this method favors the discovery of planets that are relatively close to their stars and that are very massive, i.e., hot Jupiters. Such planets would produce a more noticeable wobble in the motion of their stars.

The astrometry method, which uses astrometric observations of the wobble of the star, is mathematically similar to the Doppler shift method. From very precise astrometric observations, the slight periodic unevenness in the proper motion of the star over time is detected, and from it one can draw conclusions about the period of the planet and the radius of the star's orbit, if we know the distance to the star. Similar to the Doppler shift method, astrometry can give us the semimajor axis of the planet's orbit (from the period) and a minimum estimate of its mass, but unless we know the inclination angle, i, we cannot say more. At this time we are not aware of any planets discovered using astrometry, but it is interesting to note that attempts have been made to detect a planet around Barnard's star using this method in 1963 by Peter van de Kamp. The attempt was initially thought successful (van de Kamp claimed to have discovered a planet with mass

1.6 Jupiter masses and a period of 24 years), but it was later proved to be a false positive (Van de Kamp, P. 1963).

The most interesting method, for many people, is the direct imaging method. Direct images of an exoplanet orbiting its parent star would be a great success for current technology and would carry substantial amounts of information, which is otherwise very difficult to obtain. Unfortunately, such images of exoplanets are not yet practical in many cases, due to the small angular separation between any planet and its host star, and the enormous difference in their brightness – the planets are extremely faint compared to the stars. Even so, this method is promising and in 2004 the first image of a possible exoplanet was captured by G. Chauvin et al. (Chauvin et al. 2004). Later, in August 2005, the same group confirmed that the image was indeed that of a companion orbiting a brown dwarf star and not a background object (Chauvin et al. 2005).

Another method for detecting exoplanets is gravitational microlensing (PLANET Collaboration 2007). It uses the fact that if two distant stars happen to align briefly with Earth, the light coming from the background star will be enhanced, as if by a lens, by the gravity of the foreground star. If the foreground star has a planet, the planet's own weak gravitational field will have an effect on the light coming from the background star. OGLE (Optical Gravitational Lensing Experiment) is a project that detects exoplanets in this fashion. A disadvantage of this method is that once the stars are no longer aligned, which happens relatively quickly, it is almost impossible to do a follow-up observation using this method, because it is very unlikely that the foreground star will align with another star from the background in the foreseeable future. There have been four planets detected using this method so far (Beaulieu et al. 2006; Burgdorf et al. 2007; Gould et al.

2006; Bond et al. 2004; Schneider 2006); the first one of these four was discovered in 2004 by Bond et al.

Section 1.3: Eclipsing Systems and Transiting Exoplanets

This study is concerned with transiting extra-solar planets. Occasionally, the orbits of the star-planet system are so perfectly edge-on from Earth's point of view that the planet can be seen transiting or "eclipsing" the star. The frequency of these eclipses determines the period of the orbit, and from Newton's revision of Kepler's Third Law (knowing the mass of the star from the Hertzsprung-Russell diagram) we can find the semimajor axis of the planet (see Equation [1.2]). Since we know that the system is edge on, or nearly so, we know that the mass of the planet, which we get from Doppler shift measurements of the star's radial velocity, is the exact mass (within error), not a lower mass limit (in Equation [1.6], $\sin(i)$ becomes $\sin(i) \approx 1$).

There are two types of eclipses or transits and each of them occurs once during every orbital period. Primary transits happen when the planet crosses the face of the star and blocks part of its light, while a secondary transit is defined as the time when the planet is behind the star from Earth's point of view, and so the planet's light is blocked. Hence, during every eclipse the light output of the system will drop. The decrease of brightness of the system is more significant during primary eclipse, but it can often be measured during secondary eclipse as well.

An important property that can be measured using the fact that the planet transits the face of the star during primary transit is the radius of the planet. First, from the spectral class of the star and the Hertzsprung-Russell diagram, we can estimate the radius

of the star, R_*. Let the radius of the planet be R_p and the distance between the Earth and the star be x. Then the distance between the Earth and the exoplanet during primary eclipse is x-dx, where dx is the distance between the planet and the star during primary eclipse. Note that dx << x. Let us also assume that the star's brightness does not vary across its disk, i.e., there is no limb darkening nor are there any major stellar spots. Also, we neglect the flux from the planet (which is very small and will not have a significant effect). Look at the ratio between the star's brightness outside eclipse, I_*, and its brightness during primary transit, I_{ec},

$$\frac{I_{ec}}{I_*} = \frac{\phi\Omega_* - \phi\Omega_p}{\phi\Omega_*} = 1 - \frac{\Omega_p}{\Omega_*}, \qquad [1.7]$$

where ϕ is the flux density of the star in W/m^2·sterrad (watts per meter squared per sterradian), Ω_* is the solid angle in sterrad (sterradians) subtended by the star from Earth's point of view and Ω_p is the solid angle subtended by the planet from Earth's point of view when the planet is closest to Earth (Böhm-Vitense 1991). Note that from the definition of solid angle (Zeilik and Gregory 1998, 158) we know that

$$\Omega_* = \frac{\pi R_*^2}{x^2}, \qquad [1.8]$$

and also

$$\Omega_p = \frac{\pi R_p^2}{(x - dx)^2}. \qquad [1.9]$$

Then, we can look at the ratio of the solid angles of the star and the planet

$$\frac{\Omega_*}{\Omega_p} = \frac{R_*^2[x^2 - 2xdx + (dx)^2]}{R_p^2 x^2} = \frac{R_*^2}{R_p^2}\left[1 - \frac{2dx}{x} + \left(\frac{dx}{x}\right)^2\right]. \qquad [1.10]$$

Since the Earth-star distance, x, is so much greater than the exoplanet-star distance, dx, we can approximate $2dx/x \approx 0$ and $(dx/x)^2 \approx 0$. Hence,

$$\frac{R_*^2}{R_p^2}\left[1 - \frac{2dx}{x} + \left(\frac{dx}{x}\right)^2\right] \approx \frac{R_*^2}{R_p^2}. \qquad [1.11]$$

Equation [1.10] then becomes

$$\frac{R_*^2}{R_p^2} \approx \frac{\Omega_*}{\Omega_p}. \qquad [1.12]$$

Therefore, the ratio between the solid angles of the planet and the star is only dependent on the radii of the two objects, and if we take the reciprocal of Equation [1.12] we get,

$$\frac{\Omega_p}{\Omega_*} = \frac{R_p^2}{R_*^2}. \qquad [1.13]$$

Substituting the last result in Equation [1.7] we obtain:

$$\frac{I_{ec}}{I_*} = 1 - \frac{R_p^2}{R_*^2}. \qquad [1.14]$$

Since we know the radius of the star, R_*, from the H-R diagram, and we can measure the ratio of the intensities by direct photometric observation, we can solve for the planet's radius:

$$R_p = \left(1 - \frac{I_{ec}}{I_*}\right)^{1/2} R_*. \qquad [1.15]$$

We often define the expression $(1 - I_{ec}/I_*)$ to be the "depth of the eclipse" (Deming 2007). The presented method is a simplified version of the method used by Brown et al. (Brown et al. 2001). We assume no limb darkening of the star and that no stellar spots occur, and we don't take into account the planet's possible atmosphere or

satellites, yet this method shows the essential steps that need to be taken to determine the planetary radius.

Another interesting consequence of the transit method is the fact that some of the star's light filters through the planet's atmosphere during primary eclipse. Then, if we measure the spectrum of the star during primary eclipse, we could observe that some very weak spectral lines have appeared that are not normally present in the star's spectrum. If we subtract the usual spectrum of the star from its spectrum during eclipse, it is possible to see the remaining absorption spectrum of the upper layers of the planet's atmosphere. This was done for the first time by Charbonneau et al., who detected sodium absorption in the atmosphere of HD 209458b (Charbonneau et al. 2002). Also, recent observations analyzed by M.R. Swain, G. Vasisht and G. Tinetti found methane in the atmosphere of HD189733b (Swain, Vasisht, and Tinetti 2008).

In this study we are concerned with information that can be extracted from observations of secondary eclipses of transiting planets. The known transiting exoplanets are close to their stars – the semimajor axes are mostly between 0.02AU and 0.07AU and the typical periods are about 1 to 5 days (although HD17156b has a period of about 20 days) (Schneider 2007). Due to their proximity to the parent star, we can safely assume that such planets will be relatively hot and so they will have relatively strong thermal infrared emission, which we can hope to detect. When the star-planet system is not in eclipse we observe light from both the star and the planet and it is impossible to resolve the two objects, so photometry of the planet is impossible. However, during secondary eclipse the planet is behind the star, and we are no longer able to see the light coming from it. Even in the infrared, where the light coming from the planet is strongest, the

object's brightness is still extremely small compared to that of the star. Still, it is possible to detect the tiny drop of brightness of the system that occurs during secondary transit. This measurement was first done in 2005 by D. Deming et al. on the extra-solar planet HD 209458b (Deming et al. 2005) and by D. Charbonneau et al. on TrES-1 (Charbonneau et al. 2005). Both groups used the Spitzer Space Telescope to perform their observations.

A measurement of the brightness drop during secondary eclipse means that we know how bright the planet is, and thus we can calculate its brightness temperature – the temperature of the planet, assuming it is a blackbody, which is a reasonable approximation of its real temperature. This thesis demonstrates how this measurement of temperature is made using Spitzer Space Telescope data on the planetary system described below.

Section 1.4: Properties and Data on Transiting Exoplanet HAT-P-1b

Our analysis is focused on HAT-P-1b - a transiting exoplanet discovered in 2006 by a group led by G. Á. Bakos from the Harvard-Smithsonian Center for Astrophysics (CfA) (Bakos et al. 2007). It orbits the fainter one of the stars in the double star pair ADS 16402, namely ADS 16402B. The distance to the double star system is 139±20pc. Both stars have spectral class G0, and they are about 1550±250AU apart. The period of exoplanet HAT-P-1b is 4.46529±0.00009 days, which corresponds to a semimajor axis of 0.0551±0.0015AU (see Equation [1.2]). Its mass of 0.53 Jupiter masses was determined from Doppler shift spectroscopy using the method described in Section 1.2. The planet's radius was calculated using the method from Section 1.3 and is about 1.36±0.10 Jupiter

radii. The planet was discovered using the HATNet project, which is a wide-field survey monitoring large number of stars in order to detect transiting planet candidates by detecting the primary eclipse. The values for the mass, radius and precise period were confirmed and refined using follow-up photometric and Doppler shift observations (Bakos et al. 2007).

I have photometric data on HAT-P-1b during secondary eclipse from the IRAC (InfraRed Array Camera) instrument on the Spitzer Space Telescope. The purpose of this study is to perform photometric measurements of the change in brightness of the HAT-P-1b system during a secondary eclipse. In this thesis I will determine the brightness temperature of the exoplanet by measuring the depth of the secondary eclipse (the method for doing this will be described in Chapters 2 and 3).

Chapter 2: Data Analysis

Section 2.1: Available Data

As explained in Section 1.2, during the secondary eclipse the light from the star-planet system is expected to decrease, because the radiation coming from the planet is blocked by the star. This drop of brightness is tiny but it can be detected in the infrared part of the spectrum with enough photometric samples. By making frequent photometric observations (or samples) for about six hours - before, during and after the secondary eclipse - we can produce a light curve, which should feature a tiny drop of brightness lasting for the time of the eclipse between contacts 2 and 3[1].

My data were taken with the InfraRed Array Camera (IRAC) instrument on board the Spitzer Space Telescope. IRAC is an extremely sensitive digital camera with four detectors, optimized for infrared observations. The four detectors are designed to detect light with center wavelengths of 3.6, 4.5, 5.8 and 8.0μm (often here called "filters"; note that a separate detector is dedicated to each waveband). These are also referred to as channels 1 to 4, respectively. Channels 1 and 2 have InSb (indium antimonide) pixel arrays with working temperature of around 15K and channels 3 and 4 have Si:As (arsenic-doped silicon) arrays working at around 6K. The field of view for all channels is 5.2 arcmin on a side, and the pixel size is 1.2 arcsec on a side. All data frames have dimensions of 256 by 256 pixels (Fazio et al. 2004; Spitzer Science Center 2006). There are only three stars visible in the field – ADS 16402A, B and another one close to the

---

[1] Contact 1 is defined as the event when the planet first "touches" the limb of the star, contact 2 is the time when the planet is seen entirely inside the star, contact 3 is the time when the planet "touches" the limb of the star on the way out and starts to exit the eclipse phase and contact 4 is the time when the planet completely leaves the eclipse and no longer covers any portion of the star (see Fig. 2.5 and the explanation below).

edge of the field, which plays no role in this discussion. The data from the 4.5 and 8.0μm filters were taken on 12/28/2006, and the data with the 3.6 and 5.8μm filters were taken on 12/29/2007. The 4.5μm data (channel 2) consists of 3211 frames (or images) taken at regular intervals between 15h20m and 21h19m UT. The effective exposure time per frame was 1.2s. In the 8.0μm channel (channel 4), there were 1606 images taken also between 15h20m and 21h19m UT. The effective exposure time per frame was 10.4 s.[1] I focused my analysis on the data from the 8.0μm filter, since it is easier to calibrate than channel 2, and I still have not had the opportunity to calibrate channels 1 and 3; the observations in these channels were made only recently, at the time of this writing.

Section 2.2: Analysis Procedure

My analysis was performed in IDL (Interactive Data Language) − a scientific computer language, written for convenient and reliable analysis and visualization of data sets. IDL allows for directly typed commands and for saved routines to be executed. The data analysis was done by a series of routines that were written for this specific task. The bias, dark current and flat-field corrections were made by the Spitzer team prior to making the data available for download, so I did not need to take them into account. The star positions in the image were carefully chosen so that no known hot pixels would interfere with them, and I noticed no new hot pixels.[2]

---

[1] For more information on effective exposure time and Spitzer instrumentation in general, please refer to the Spitzer Observer's Manual version 8.0, released by the Spitzer Science Center on 08/15/2007. At the time of this writing, it is accessible at http://ssc.spitzer.caltech.edu/documents/som/som8.0.pdf.
[2] Further information on bias, dark field and flat field subtractions, and bad pixel handling, is available again in the Spitzer Observer's Manual. For a more general reading on astronomical imaging, refer to "Handbook on CCD Astronomy", Howell, S.B., 2000.

I started by cleaning up the cosmic rays in the images. The term "cosmic rays" here refers to high energy particles, which when they hit the camera during exposure are seen in the image as bright dots or bright narrow streaks (see Figure 2.1). Since the cosmic ray is a single particle, it would appear only in one image, but never in multiple ones. Cosmic rays are not related to the source, and therefore are an effect on the image,
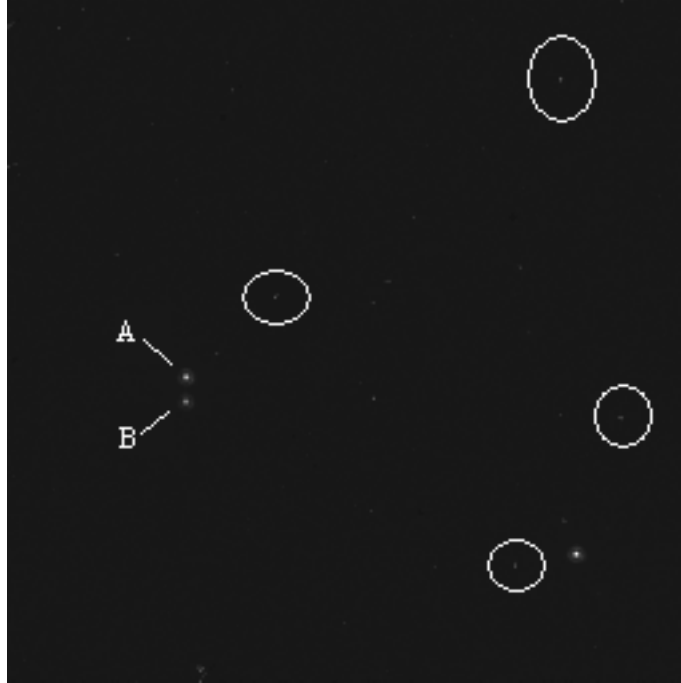
Figure 2.1: *A typical data frame before cleaning the cosmic rays, with some of the more prominent ones circled. ADS 16402A and B are shown. Exoplanet HAT-P-1b orbits star B.*

which I needed to correct for. Since the frames are arranged chronologically, I was able to take a time series for every pixel in the camera, i.e., I noted how its value changed as a function of time in all images. Let us consider a pixel with coordinates on the camera array (x, y). In general, for any frame, N, where N is the time-ordered index number of the frame, I compared the image pixel (x, y) in N with the pixel (x, y) in frames N-2, N-1, N+1 and N+2. I took the median of the pixel (x, y) in the five frames, N-2, N-1, N, N+1, N+2, and if the value of this pixel in frame N exceeded 1.7 times the median, I

assumed that it had been hit by a cosmic ray and set its value to be equal to the median. I assumed threshold of 1.7 times the median, since this value results in the best outcome - no pixels without definite cosmic ray hits were cleaned, and no obvious hits were missed. Of course, in this scenario, pixels from the first two and the last two frames are problematic since at least one of the frames N-2, N-1, N+1 and N+2 does not exist for them. My solution was to compare the pixel (x, y) from frame 1 with the pixel (x, y) from frames 2, 3, 4 and 5 and to compare the second frame's pixel (x, y) to pixels from frames 1, 3, 4 and 5. Symmetrically, the last frame's pixel (x, y) was compared to the previous four images' pixel (x, y), and the pixel (x, y) in the second-to-last frame to the (x, y) pixel in the three images before the second-to-last and the last image. This procedure was performed for all pixels (x, y) which were going to be included in the photometric measurement of the star. The rest were irrelevant, since the background estimation method was immune to cosmic rays, as described below. Note that this method allows the pixels in the data to change gradually in brightness with time, but detects any sharp peaks caused by cosmic rays. On the other hand, if I had taken the median of the values of the same pixel through all frames (i.e., over the whole time series), I would have missed some cosmic rays - the pixels may gradually increase their brightness (due to reasons to be discussed below) and therefore I would have had to set the threshold much higher, in order not to "clean" the good pixels that are brighter than the rest, thus allowing some cosmic rays to remain undetected in the dimmer pixels.

My next step was to perform photometry on the star ADS 16402B – the star around which the planet HAT-P-1b orbits. During the course of the observation session the position of the star on the pixel array does not change significantly (the drift is about

0.2 pixels, measured by the drift of the Gaussian center of the star). For every image I determined a 9 by 9 square aperture of pixels, centered on the pixel that appears to be the brightest in the image of the star ADS 16402B in many of the frames (see Figure 2.2).
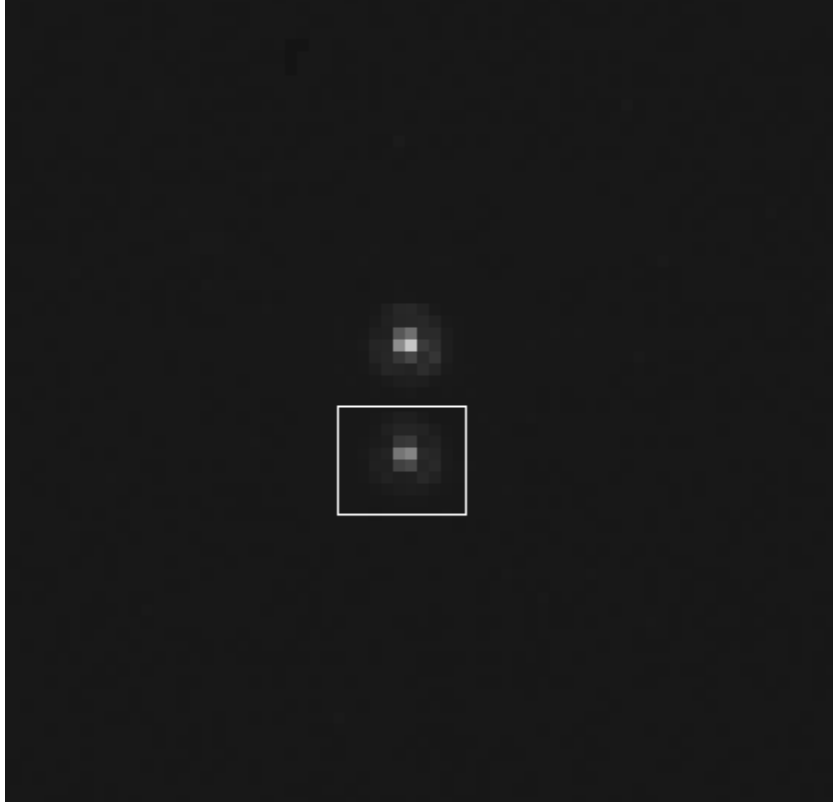
Figure 2.2: *This figure shows the 9 by 9 pixel photometric aperture around ADS 16402B. This is a magnified view of the same image as Figure 2.1, with the square aperture imposed and cosmic rays cleaned.*

The size of the 9 by 9 box was chosen so that it includes a maximum amount of pixels without overlapping with the point spread function of the neighboring brighter star of the pair (the separation between the centers of the two stars was 10 pixels). For every frame, I summed all the pixel values in the 9 by 9 pixel box and subtracted the estimated background radiation per pixel multiplied by the number of pixels in the aperture, 81. This gave me the photometric value of the star. The background radiation per pixel was estimated by making a histogram for every frame – I plotted pixel value on the x-axis and

the number of pixels with that value on the y-axis. Since the vast majority of pixels in any frame are only detecting background radiation, on the histogram there is a very prominent peak at this "background" level (see Figure 2.3). Note that this method of determining the background radiation levels is not affected by cosmic rays or a small number of stars in the field – they just do not cover enough pixels to be prominent features in the histogram. The source code of the IDL routine written to clean the cosmic rays and to perform photometry is shown in Section A1 in the Appendix. For the background estimation function source code see Section A2.
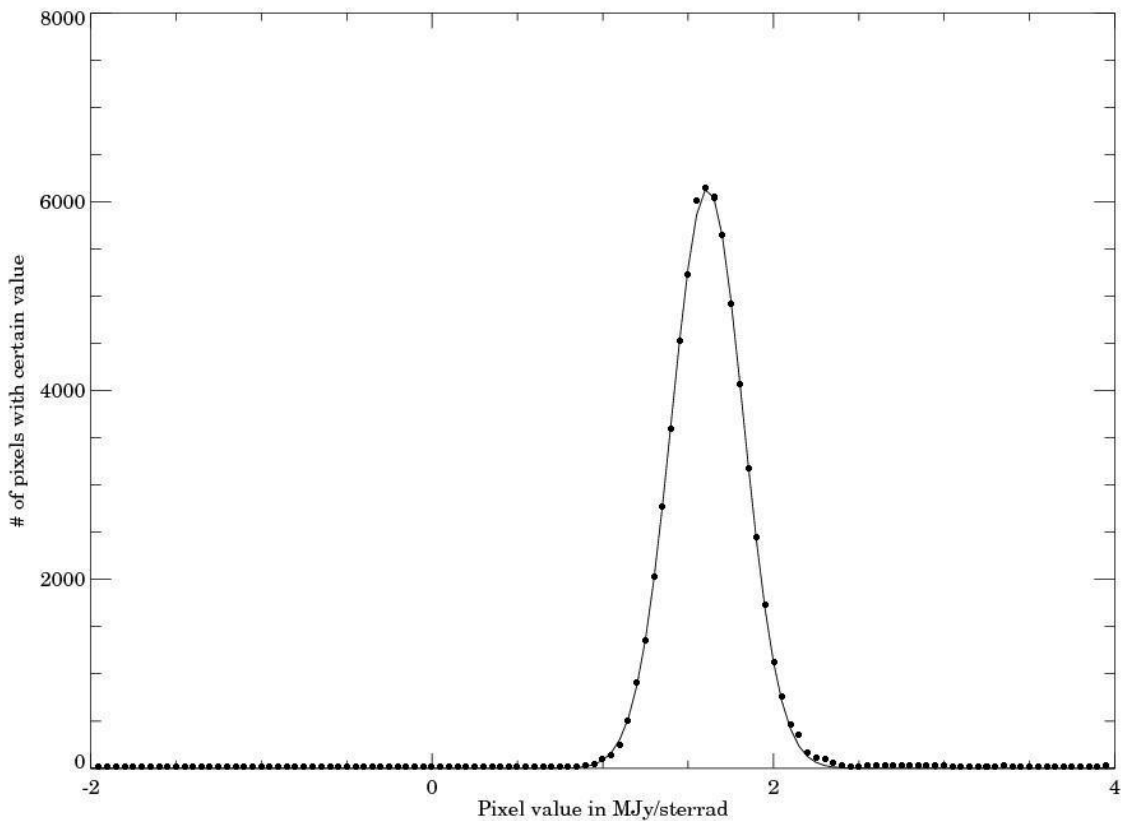
Figure 2.3: *This graph shows the number of pixels versus the pixel value. The actual values are represented by dots and the best Gaussian fit is shown as a line. The number of pixels that have value bigger than 4 is very small and is not shown on the graph. The size of the binning intervals along the pixel value axis is 0.05 MJy/sterrad. From the graph it is clear that the background level is around 1.5 MJy/sterrad (which is the peak of the Gaussian feature) for this frame.*

I constructed the initial light curve for the 8μm filter by plotting the brightness of the star versus time. The time scale on the x-axis was represented in terms of phase – a system where phase 0.00 corresponds to the middle of the primary transit (or eclipse), and the other points are fractions of the time passed until the next primary transit. In this way, 0.50 is the middle of the secondary eclipse, for a circular orbit. The exact phase for the secondary eclipse depends on the eccentricity and inclination of the planet's orbit relative to the line of sight from Earth.
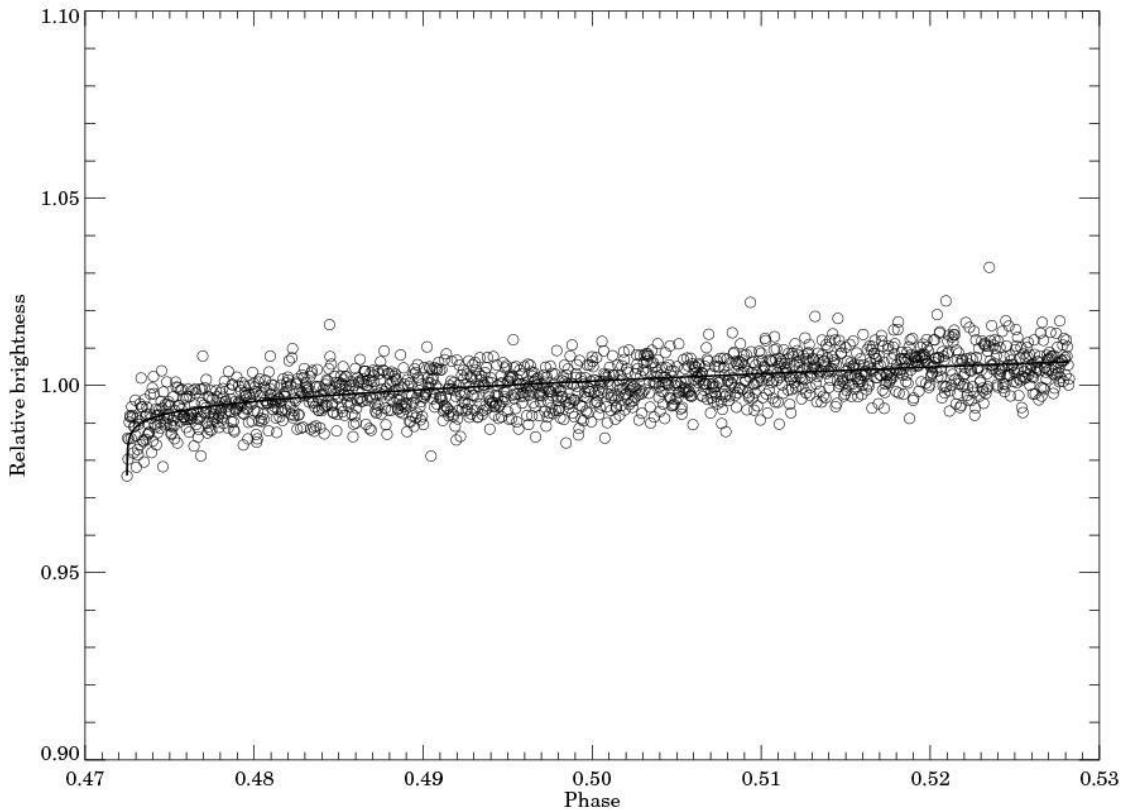
Figure 2.4: *This figure represents the photometric data points divided by their average and plotted against time in terms of phase. 0.50 is the middle of the calculated secondary transit (using* Bakos et al. 2007*). The brightness is given as a fraction of the average brightness. The baseline is shown as a dark line.*
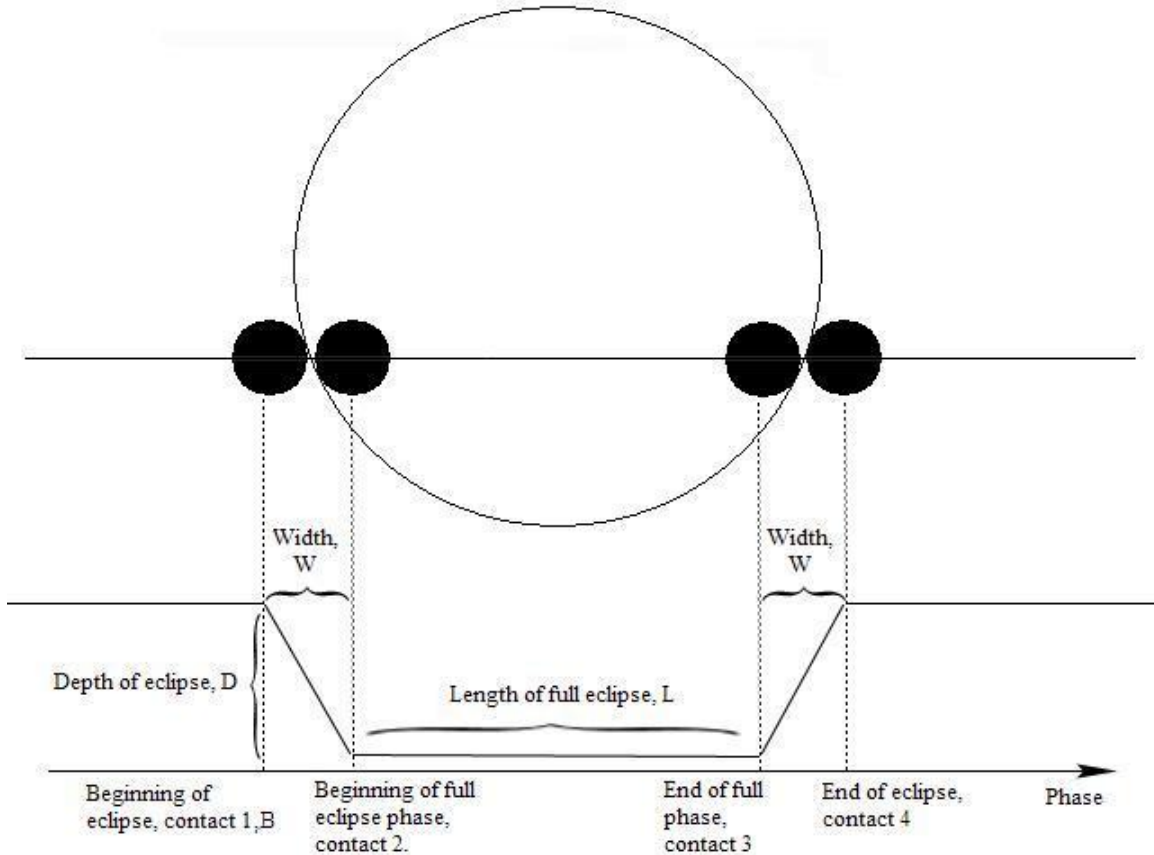
Figure 2.5: *This is a schematic representation of my eclipse model. The parameters used in the fitting procedure and the important moments of the eclipse are marked. My model is similar to that of Brown et al. (Brown et al. 2001) but differs at the bottom of the eclipse curve (the line segment L), which here is flat, and not curved, since we are looking at a secondary eclipse and during the time L (or "full eclipse" of the planet) we cannot see the planet at all, only the constant flux from the star.*

The photometric values of the star are plotted on the y-axis. I divided them by their average in order to achieve a unitless quantity – a fractional difference from the average flux (see Figure 2.4). I noticed a strong tendency for the star to look brighter as the observation session proceeded. This is a known, and expected, phenomenon, commonly seen in observations with IRAC and other Spitzer instruments. During the course of the observations, the objects would often begin to look brighter in a non-linear fashion. The reason for that behavior is not entirely clear, but it is thought that this is due to potential wells, or "electron traps," in the detector pixels, which capture many

photoelectrons from the first exposures thus making the star look dimmer early in the observing session. However, as the observations proceed, these potential wells are filled with electrons and they can no longer capture new ones, and thus more electrons are read out by the electronics and the image of the star appears to become brighter. I accounted for this effect by fitting a sum of a linear and a logarithmic function to all data (a baseline) that was not part of the eclipse (which is noticeable with close scrutiny in Figure 2.4 as a slight dip in the data around a phase of 0.50). In order to achieve a flat light curve in which the eclipse would be prominent and easy to quantify, I subtracted this baseline (shown in Figure 2.4) from the data (Deming 2007). The source code for the baseline fit and subtraction is presented in Section A3.

An eclipse model curve was created to be fitted to the data. The points at which the planet is shown in Figure 2.5 are called contact points and are chronologically numbered from 1 to 4. The model relied on the following parameters – beginning phase of the eclipse (or contact 1), width of the areas where the brightness was increasing or decreasing rapidly (i.e., times between contacts 1 and 2 and contacts 3 and 4), length of the full eclipse and, most importantly for this survey, depth of the eclipse as a fraction of the mean brightness level (B, W, L and D respectively in Figure 2.5). My eclipse model, as shown in Figure 2.5, connects with straight lines the intensity of the star-planet system at these points, which is a reasonable approximation.

The depth of the eclipse was determined by χ^2 (chi-squared) minimization. χ^2 is defined as

$$\chi^2 = \sum_{i=1}^{n} \frac{(x_i - m_i)^2}{\sigma_i^2}.$$ [2.1]

In the equation above, x_i is the ith measured value, m_i is the ith model data point and σ_i is the error for the ith measured point (Taylor 1997). The chi-squared minimization method uses the χ^2 statistic to make an estimate of how well a model fits the data - the smaller χ^2 is, the better the fit (Press et al. 1992, 657). Generally, a large number of parameter values for the model are tried and the one which achieves smallest χ^2 is considered the best fit. I wrote a routine (see Section A4 in the Appendix) to try one million combinations of the parameters B, W and L – i.e., 100 values for B times 100 values for W times 100 values for L. Notice that no assumptions were made about the depth of the eclipse, D. Again using χ^2 minimization, the best fit depth of the eclipse was calculated separately for each one of the combinations of B, W and L. Thus, a complete model light curve (i.e., a set $\{m_i\}$) was created for every combination of B, W and L values. The goodness of fit (or χ^2) of each set $\{m_i\}$ was compared to the χ^2s of all other model light curves. Finally, the one with the smallest χ^2 was chosen to be the best fit eclipse curve. The smallest χ^2 determination of D is the result reported in Chapter 3 and is used in all calculations presented there.

Section 2.3: Error Analysis

The error analysis relied on a simulation of possible data sets. Specifically, I used a version of the "bootstrap" Monte Carlo method. The bootstrap Monte Carlo method is described in Press's Numerical Recipes in C. The variation used here, in general, consists of taking the differences between the measured values in a data set and the corresponding best estimate model values, randomly scrambling these differences and adding them back to the best estimate model values in their original order. An arbitrary number of "fake"

data sets can be simulated in this fashion. This way, new sets of data points are produced. For each new set the same analysis that was done on the original data set has to be performed.

The bootstrap method is a powerful technique in cases like the present one, where the precise distribution of the errors is not well-known, so synthetic data sets cannot be simulated using regular Monte Carlo simulation. Bootstrap Monte Carlo is an accepted method and there is enough proof for its reliability (Press et al. 1992, 691-692, and references therein). It is important that the points in the original data set are distributed independently (i.e., the values of the points do not depend on each other) and identically (i.e., the distribution of the points does not change over time, for example from Gaussian to Poisson). Additionally, one has to make sure that the points are not rearranged in some specific order during the analysis. If any of these conditions is violated, the method will likely fail. If these assumptions are not violated, the synthetic results from the generated "fake" data sets can be used to determine confidence limits for the parameter we are interested in (Press et al. 1992, 689-691).

For the data set that we have, consisting of the relative brightness of HAT-P-1b over time, it can be safely assumed that the distribution does not change significantly over time, and that the points are independent. Also, the analysis performed did not use any rearrangements of data points and so it was safe to use bootstrap Monte Carlo simulation of synthetic data sets. I took the differences of the real data to the best fit eclipse curve. These differences were then randomly scrambled and added to the best fit model in order to create a "fake" data set. In this fashion I simulated one thousand "fake" data sets, for statistical significance. For each one of them the same procedure described

in Section 2.2 was applied (see Section A6 for source code). The average depth of the thousand simulated eclipses was calculated and it was found to coincide remarkably well with the best fit model depth found using the procedure from Section 2.2. I used the standard deviation of this average as a random error estimate for the best estimate eclipse depth. While this method of error analysis can be improved - systematic errors need to be taken into consideration - the presented procedure gives a good estimate of the uncertainties involved.

Chapter 3: Results and Conclusion

Section 3.1: Results

After fitting the eclipse model to the data, and performing the error analysis as described in Chapter 2, I measured an eclipse depth of 0.17±0.03% (or 0.0017±0.0003). This value is an expression of how much the brightness of the system decreases during secondary eclipse compared to its brightness outside of eclipse. These results are illustrated with the light curves and model plots shown in Figures 3.1 and 3.2. Figure 3.1 is a plot of the relative brightness of the star for all 1606 images taken in the 8.0 μm filter of the IRAC instrument the Spitzer Space Telescope. The brightness measurements are plotted against phase and no individual error bars have been plotted since they would be too big (on the order of 0.002) and make the plot cluttered and hard to interpret. On the same figure I have also plotted the best estimate curve, which is shown as a solid line. The eclipse curves that have eclipse depths one standard deviation (or 1σ) from the best estimate curve are shown with dashed lines below and above the best fit curve. The 1σ eclipse depths are 0.0020 and 0.0014. Even though the computer algorithms easily detect the eclipse, for the human eye this is difficult to do just by looking at Figure 3.1. To make the drop of brightness easier to see, I have plotted the averages of every 20 data points from Figure 3.1 in Figure 3.2. The best estimate eclipse curve and the curves designating the one standard deviation uncertainties are also shown for comparison with Figure 3.1. The IDL code used to generate Figure 3.2 is shown in the Appendix, Section A7.
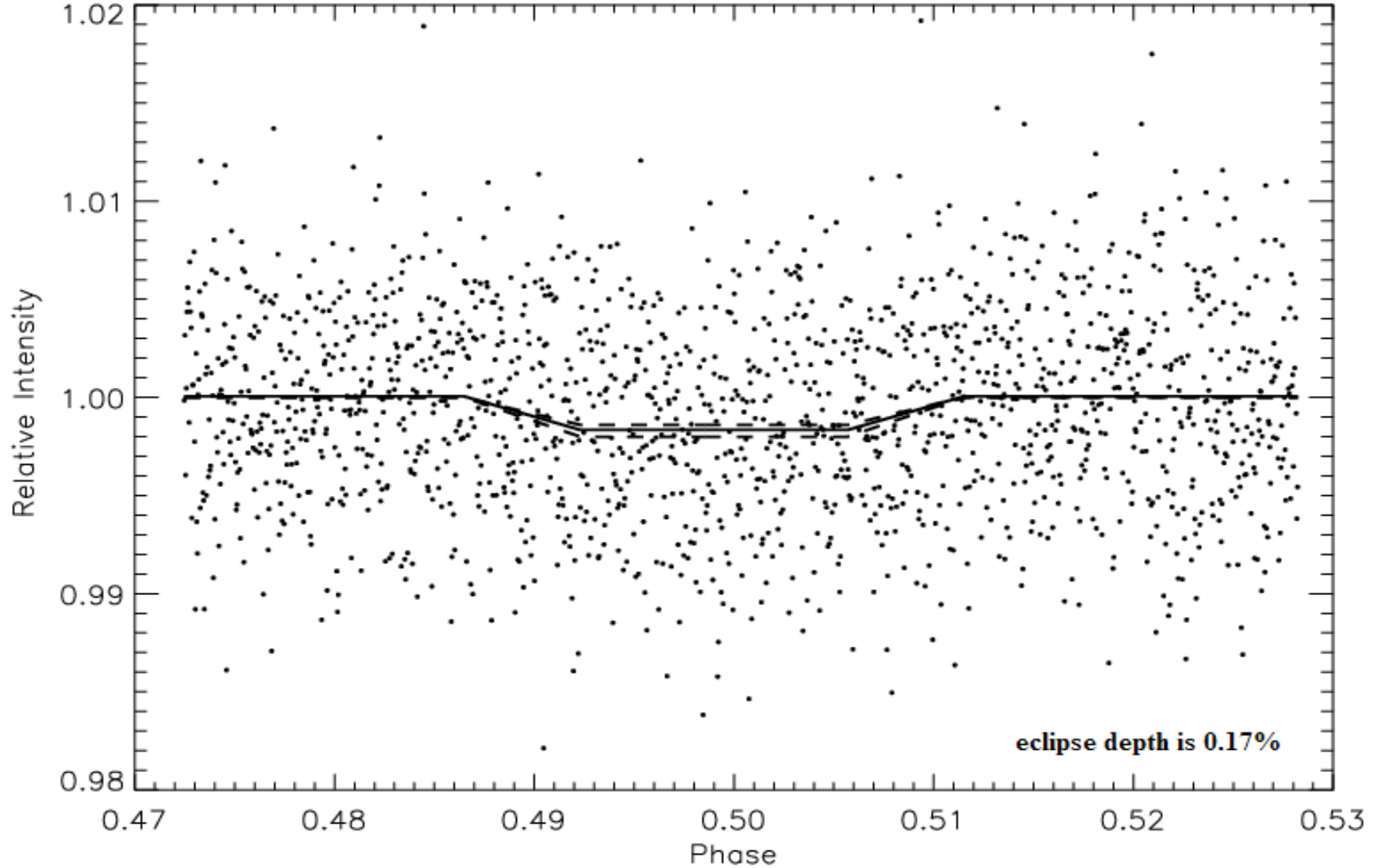
Figure 3.1: *The figure above shows the brightness of the star-planet system on the y-axis and the phase of the eclipse on the x-axis. The brightness is represented as a fraction of the average brightness of the system outside eclipse. The solid black line represents the best fit eclipse curve and the dashed lines represent the 1σ deviations from the best fit. For the best estimate eclipse the decrease in brightness is 0.17% from the average, and the 1 σ uncertainties are 0.03%. No errors for the individual data points are plotted.*
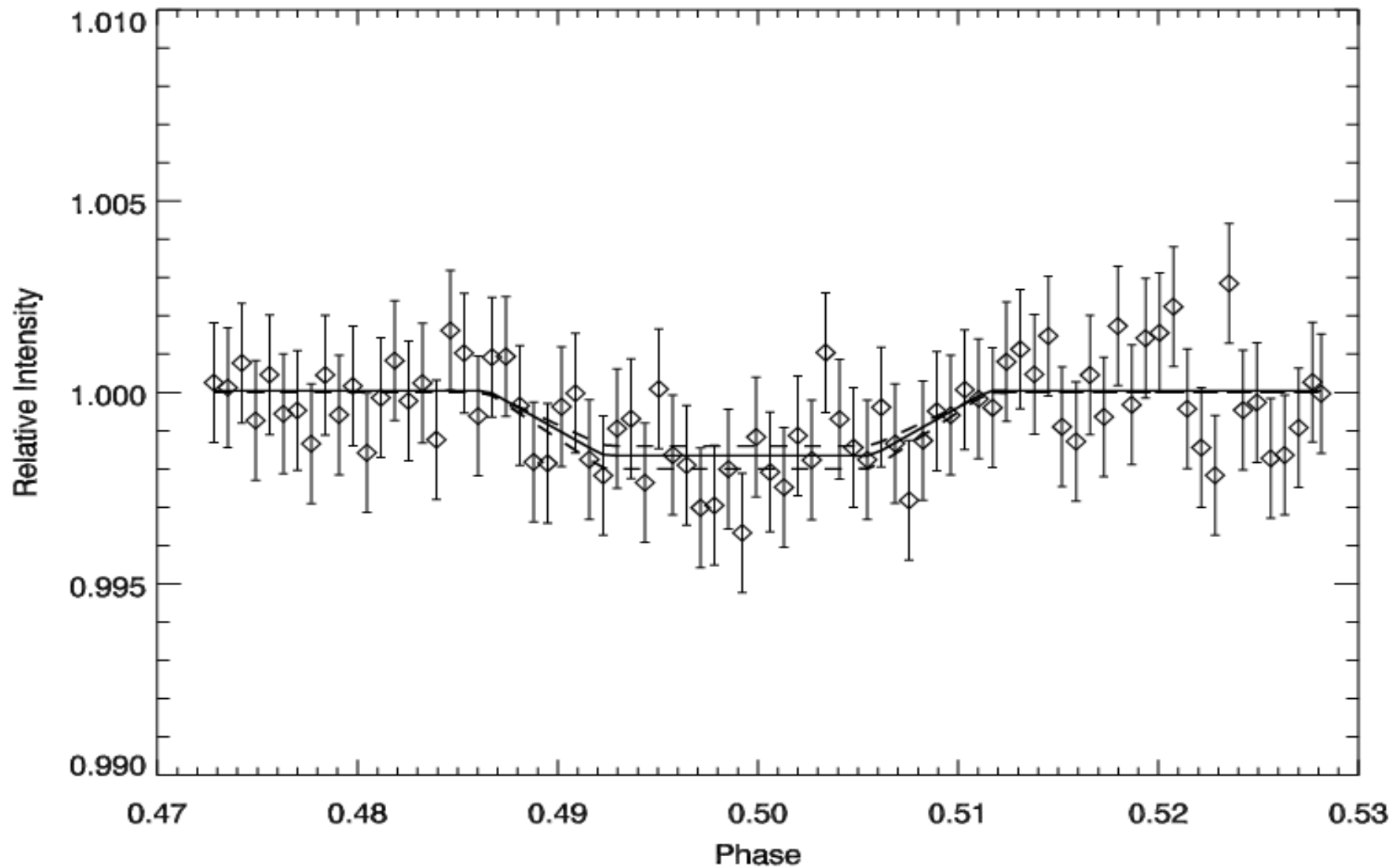
Figure 3.2: *In this graph I have averaged (or binned) the brightness points shown in Figure 3.1. Every 20 points are averaged and the resulting points are plotted against the phase of the eclipse. Again, the brightness is expressed as a fraction of the average brightness outside eclipse. The error bars shown are the standard deviations of the individual bins. Note that the eclipse is much more easily seen than in Figure 3.1. IDL source code used to bin the data can be found in A7.*

In order to convert the eclipse depth to the brightness temperature of the planet we use a method outlined by David Charbonneau et al. and Drake Deming et al. (Charbonneau et al. 2005; Deming et al. 2005). Consider the total flux of the planet-star system outside eclipse, ϕ_t, which is equal to the sum of the flux of the planet, ϕ_p, and the flux of the star, ϕ_*, or

$$\phi_t = \phi_p + \phi_* = \Omega_p B_p + \Omega_* B_*, \qquad [3.1]$$

where Ω_p is the solid angle subtended by the planet in sterrad, Ω_* is the solid angle subtended by the star in sterrad, B_p is the brightness of the planet in J/m^2·s·sterrad (Joules per meter squared per second per sterradian) and B_* is the brightness of the star in J/m^2·s·sterrad. The flux of the system must drop by $\Omega_p B_p$ during secondary eclipse (since we do not see the planet's flux at this time) and the total brightness outside the eclipse is $\Omega_p B_p + \Omega_* B_*$. Therefore, the depth of the eclipse as a fraction of the brightness outside the eclipse, D, is

$$D = \frac{\Omega_p B_p}{\Omega_p B_p + \Omega_* B_*}. \qquad [3.2]$$

We already know the depth of the eclipse and we can easily convert it to brightness temperature of the planet in the following way. From Planck's blackbody radiation formula we know that

$$B_* = \left(\frac{2h\nu^3}{c^2}\right)\left(\frac{1}{e^{h\nu/kT_*} - 1}\right), \qquad [3.3]$$

and

$$B_p = \left(\frac{2h\nu^3}{c^2} \right)\left(\frac{1}{e^{h\nu/kT_p} - 1} \right).$$ [3.4]

In Equations [3.3] and [3.4], ν is the frequency of light in Hertz (Hz) in which the eclipse was observed (in our case the wavelength is 8µm, which corresponds to $\nu = 3.75 \cdot 10^{13}$Hz), T_p is the brightness temperature of the planet in Kelvin (K), T_* is the brightness temperature of the star in K, h is Planck's constant in m^2kg/s (meter squared times kilogram per second), k is the Boltzmann constant in J/K (Joules per Kelvin), and c is the speed of light in meters per second. We can easily solve Equation [3.4] for T_p to obtain:

$$T_p = \frac{h\nu}{k \ln\left(\frac{2h\nu^3}{c^2 B_p} + 1 \right)}.$$ [3.5]

Equation [3.5] is an expression for the brightness temperature of the planet, but we need a way to calculate B_p. In order to do that we first take the reciprocal of Equation [3.2]:

$$\frac{1}{D} = 1 + \frac{\Omega_* B_*}{\Omega_p B_p}.$$ [3.6]

Recall from Equation [1.12] in Section 1.3 that

$$\frac{R_*^2}{R_p^2} \approx \frac{\Omega_*}{\Omega_p}.$$ [3.7]

Therefore, we can substitute Equation [3.7] in Equation [3.6] and solve for B_p to obtain

$$B_p = \frac{DB_*}{1 - D}\left(\frac{R_*}{R_p} \right)^2.$$ [3.8]

We know the value of B_* from Equation [3.3], and we have an estimate of R_* from the Hertzsprung-Russell diagram. R_p was found using the method described in Section 1.3 by the team that discovered HAT-P-1b. Equation [3.8] gives an estimate of B_p that can be

used to obtain a value for the brightness temperature of the planet, T_p (Equation [3.5]). For my temperature estimate I used the planetary and system parameters presented in Table 3.1. This table shows all the parameters needed to perform the brightness temperature calculation. These values (except the secondary eclipse depth and the frequency) were determined by the discovery paper for HAT-P-1b (Bakos et al. 2007).

Parameter	Value
R_p	$1.36 \pm 0.10\ R_J$
R_*	$1.15 \pm 0.10\ R_{Sun}$
T_*	5975 ± 45 K
D	0.0017 ± 0.0003
ν	$3.75 \cdot 10^{13}$ Hz

Table 3.1: *The table shows all parameters necessary to determine the brightness temperature of the planet. R_p, R_* and T_* are taken from the discovery paper by Bakos et al. in 2007, and D is my result for the depth of the secondary eclipse. The unit R_J stands for Jupiter radii and the unit R_{Sun} stands for solar radii.*

If the best estimate values for R_p, R_*, T_* and D are used, the calculations (Equations [3.5] and [3.8]) yield $T_p = 1290$K. The uncertainty of T_p had to be estimated, so I varied R_p, R_* and D and looked at the resulting brightness temperatures. The 45K uncertainty on the brightness temperature of the star has very little effect on the calculation, and therefore, for simplicity, the best estimate of 5975K for T_* was used in all calculations mentioned below. If the minimum value of R_p and the maximum values of R_* and D are used, in order to maximize the result, the calculations return T_p of 1700K. The minimum result is achieved by calculating the temperature using the lower

limit for D and R_p and the upper limit for R_*. In this case the planet's temperature is 990K. I performed the brightness temperature calculations for all combinations of lower, upper and best estimate values for the three important parameters, D, R_* and R_p. The resulting 27 brightness temperatures had a mean of 1300K and a standard deviation of 170K, and thus my final result for the brightness temperature is 1300±170K. This approach gives a reasonable estimate of T_p and of the random error in T_p even though it is not a complete error analysis. The result needs to be rechecked by continuously varying T_*, and by continuously varying D, R_* and R_p within the 1σ uncertainties, not by just taking the best estimate values and the extreme values.

Section 3.2: Conclusion and Discussion

In this thesis I calculated the brightness temperature of HAT-P-1b for a wavelength band centered on 8.0μm. The calculated value of 1300±170K for the planet's brightness temperature is somewhat expected, since a planet so close to its star it is certain to be relatively hot (hence the name of the class of large planets close to their stars – "hot Jupiters"). The importance of the result can be understood if we remember that "brightness temperature" is the temperature of an object, calculated from its flux, assuming that this object is an ideal blackbody. However, our planet is *not* an ideal blackbody, and therefore, the brightness temperature is a convenient measure of the flux output of the planet in a certain band-pass. In addition, even though the physical temperature of the planet will deviate from the brightness temperature due to absorption and emission features in the spectrum, it is not unreasonable to assume that these two

quantities do not differ significantly. Thus, the brightness temperature of the planet is a reasonable estimate of its physical temperature.

If the brightness temperature is measured for HAT-P-1b in multiple band-passes, we will have flux measurements in a number of different wavelengths. Thus, we can plot the brightness temperatures versus the wavelengths in which they were obtained and we will essentially have a crude broadband spectrum of the planet. We certainly will not be able to distinguish individual spectral lines, but we will be able to see the large-scale features of the spectrum. Since the flux of any gas giant planet comes from its atmosphere (reflected light from the host star or blackbody radiation from the planet itself), this crude spectrum will allow us to draw conclusions about the chemical composition of the upper layers of HAT-P-1b's atmosphere. We will be able to compare the measured broadband spectral features with existing theoretical models for the spectrum of the planetary atmosphere. Ultimately, our goal is to create such a spectrum for HAT-P-1b using the data that we have from Spitzer Space Telescope at center wavelengths 3.6, 4.5 and 5.8μm (IRAC channels 1, 2 and 3) and the present result coming from data at center wavelength of 8.0μm. The yet-unprocessed data will be analyzed as described in Chapter 2 this summer to give us four estimates of the brightness temperature of the planet at the four wavelengths mentioned above. We will compare the spectrum with theoretical models for the atmosphere of the planet. We hope to be able to reject some of them, depending on how well they match with the observed broadband spectrum. There is a chance that we will be able to confirm some of these models.

Additionally, since the atmospheric transparency of the hot Jupiters for different wavelengths changes with height, the flux in these wavelengths will predominantly come

from different heights above the "surface" (or distances from the center of the planet). In this way we will estimate the temperature of the atmosphere of different layers and there is a chance that we may find a temperature inversion (lower layers are colder than upper layers). A temperature inversion was first found in an extrasolar planet in 2007 (Knutson et al. 2008). By continuing this research we will expand our knowledge on the temperature structure and the chemical composition of the atmosphere of HAT-P-1b and of hot Jupiters in general.

Appendix A: IDL Routines Used

In order to perform the analysis described in Chapter 2 I implemented IDL routines (or scripts). I wrote seven routines and they are presented in this Appendix. Additionally, I used the standard IDL routine library, the IDL Astronomy User's Library and a scrambling routine by R. Sterner. All routines used, except the ones I wrote, are freely available on the web (see A8 for URLs).

The routines written by me could have been part of one large script, but for the purposes of debugging it was convenient to separate them into reasonably small sections. The scripts presented here form a sort of a pipeline – the first routine reads the data and begins the analysis, the intermediate routines perform most of the analysis and the last routine returns the depth of the best fit eclipse and its uncertainties. The dependence of the routines is shown in Figure A.1 below.
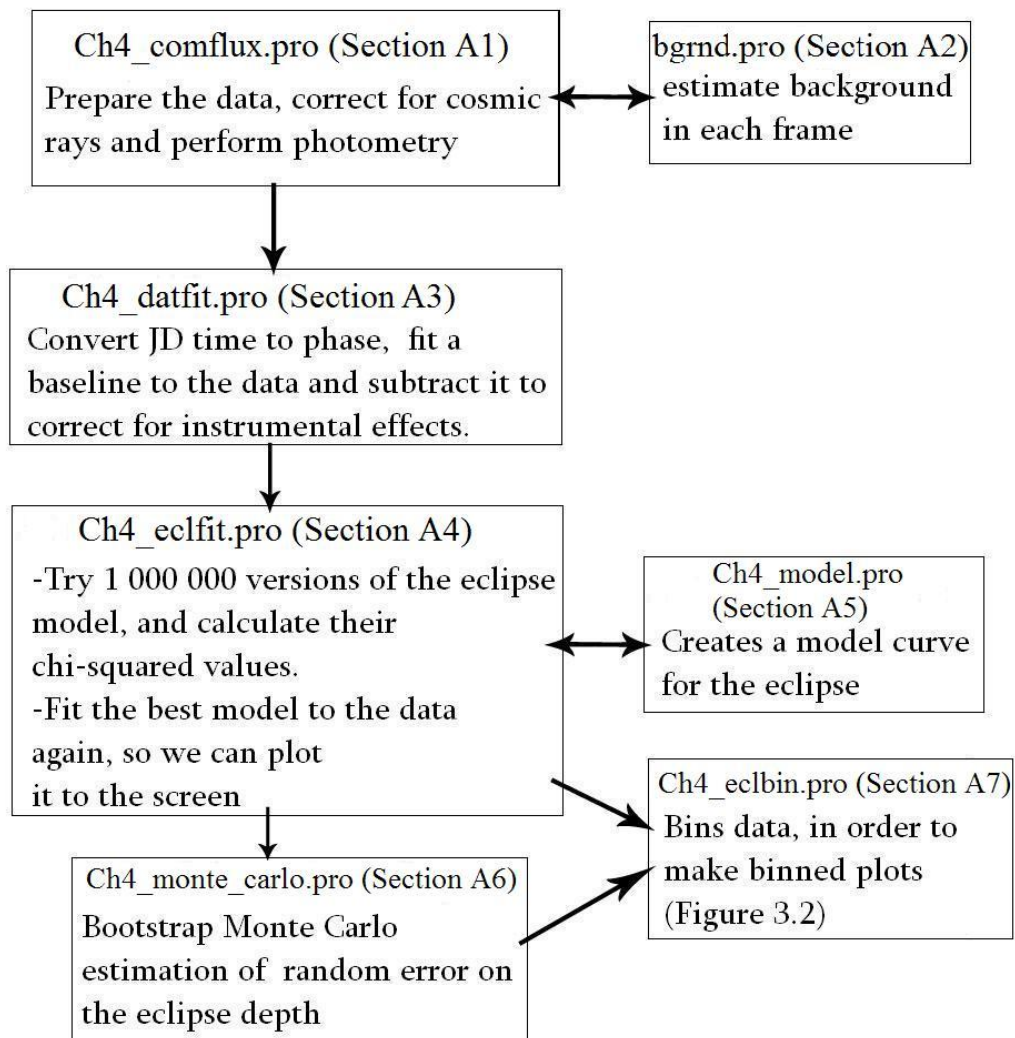
Figure A.1: *The chart above presents the flow of the data through the routine pipeline. The scripts are indicated with their section number in this Appendix, and their routine filename. A short description of the tasks of each script is also provided. Scripts A2 and A5 are called from within A1 and A4 respectively, while A7 is optional and takes the results from A4 and A6.*

Section A1: Data Preparation and Photometry Routine

Routine: CH4_COMFLUX.PRO
Purpose: Prepare the data for analysis, clean the cosmic rays and perform photometry

```
nfrpos = 1606      ;number of frames per position of the star on the array
nfrall = 1606      ;number of frames total
xsz    = 256       ;x size in pixels
ysz    = 256       ;y size in pixels

xpos1  = 67        ;x position of the "upper star" on the
                   ;array (dimmer star)HAT1
ypos1  = 150       ;y position of the "upper star" on the
                   ;array (dimmer star)HAT1
xpos2  = 67        ;x position of the "lower star" on the
                   ;array
ypos2  = 140       ;y position of the "lower star" on the
                   ;array

flux1  = make_array(nfrpos,2, /double)
;flux-in-time array of Star1

flux2  = make_array(nfrpos,2, /double)
;flux-in-time array of Star2

time0  = make_array(nfrpos, /double)
timeall= make_array(nfrall, /double)

bg1a   = make_array(nfrpos, /double)

;DATE-OBS is the header keyword needed
yr = 2006d  ;year
mn = 12d     ;month
dy = 28d     ;day
rjd= 0d      ;reduced JD

x0 = 4.     ;photometry pixel box is 1 + 2*x0
y0 = 4.     ;no more than 4, else PSFs overlap
frame= 0
x    = 0
y    = 0
a    = make_array(nfrpos,xsz,ysz)
otstr= make_array(nfrpos,/string)
;observation time as a string
otrjd= make_array(nfrpos,/double)
;observation time in decimal hours, after midnight on UT

date = make_array(6,  /double)
fp   = '/---/---/data/HAT-P-1b/bcd'
farr = file_search(fp,'*bcd.fits')

;*****READ THE FITS FILES INTO A DATA CUBE*****

FOR frame = 0,nfrpos-1 DO begin
    im          = readfits(farr(frame),head,/silent)
    otstr[frame] = strmid(head[28],22,12)
```

```
;the time as a string from the right header keyword
    hrs          = strsplit(otstr[frame],':',/extract)
;actually, hrs is[hours min sec] array
    hh           = double(hrs[0])
    mm           = double(hrs[1])
    ss           = double(hrs[2])
    date         = [yr,mn,dy,hh,mm,ss]
    juldate, date, rjd
;reduced julian date =>add 2400000 to get JD
    rrjd         = rjd - 54050d
;subtract 54 050 from the reduced Julian date
;to show more significant digits on the plot
    otrjd[frame] = rrjd
    a[frame,*,*] = im[*,*]
ENDFOR


;*******CLEAN UP COSMIC RAYS******

frame = 0
FOR frame = 0,nfrpos-1 do begin
for  x = xpos1-x0,xpos1+x0 do begin
   for y = ypos1-y0,ypos1+y0 do begin
     if (frame eq 0)or(frame eq 1) then begin
      if a[frame,x,y] gt 1.7*median(a[0:4,x,y]) then begin
          a[frame,x,y] = median(a[0:4,x,y])
       endif
      endif

      if(frame eq nfrpos-1)or(frame eq nfrpos-2) then begin
       if a[frame,x,y] gt 1.7*median(a[0:4,x,y]) then begin
         a[frame,x,y] = median(a[0:4,x,y])
       endif
      endif

      if (frame ge 2) and (frame le nfrpos-3) then begin
       if a[frame,x,y] gt 1.7*median(a[frame-2:frame+2,x,y]) then begin
         a[frame,x,y] = median(a[frame-2:frame+2,x,y])
       endif
      endif
    endfor
endfor
ENDFOR

;*****PHOTOMETRY PART*****
; also, here the time is tagged to each photometry value

time0    = otrjd   ;time is the same for both stars!
for frame = 0,nfrpos-1 do begin
    totflux1 = 0.  ;signal value at this image -Star1
    totflux2 = 0.  ;signal value at this image -Star2
    bg1      = 0.  ;background is the same for both stars!

    totflux1 = total(a[frame, xpos1-x0:xpos1+x0, ypos1-y0:ypos1+y0])
;    totflux2 = total(a[frame, xpos2-x0:xpos2+x0, ypos2-y0:ypos2+y0])

    ;background correction:
    dummy = bgrnd(a,frame,bg1)
```

```
    bg1a[frame]  = bg1
    flux1[frame,0] = totflux1 - bg1*(n_elements(a[frame, xpos1-$
                                  x0:xpos1+x0,ypos1-y0:ypos1+y0]))
    flux1[frame,1] = time0[frame]
;   flux2[frame,0] = totflux2 - bg1*(n_elements(a[frame, xpos2-$
                                  x0:xpos2+x0,ypos2-y0:ypos2+y0]))
;      flux2[frame,1] = time0[frame]
endfor

;*****PLOT RESULTS*****

plot,flux1[*,1], flux1[*,0]

;*****SAVE VARIABLES*****

save, filename='ch4_comflux.sav'

end
```

Section A2: Background estimation function
Function: BGRND.PRO
Note: This function is called from inside CH4_COMFLUX.PRO (see Section A1).
Purpose: Estimate the background of the image using a histogram and Gaussian fit, as
  described in Section 2.2.

```
function bgrnd, a, frame, avbg

;******background estimation******
;based on a histogram graph - the most numerous pixel value
;represents the average background.


binsz = 0.05d        ;binsize for the histogram - what difference in
                          ;value corresponds to 1 division.
hmin  = -5               ;minimum value to be considered by the histogram
hmax  =  5               ;maximum value to be considered by the histogram

h = histogram(a[frame,*,*],binsize=binsz, /NAN, min=hmin,max=hmax)
x_gauss = findgen(2000)
g=gaussfit(x_gauss[0:n_elements(h)-1],h, a_coeff, nterms=3, chisq=chisq)

                                                                ;we
  add 0.5 to the center, because
avbg     = (a_coeff[1]+0.5)*binsz+hmin    ;the center is only the
  beginning
                                                                ;of
  the binsz interval, and 1 is

  ;the length of the binsz interval
;*****NOTE:*****
;We multiply by binsz because 1 division of the plot corresponds to binsz
;difference in value. We add hmin, because on the plot, the values
;start from 0, but our real values start from hmin.
```

```
;a_coeff[0] is the height of the Gaussian,
;a_coeff[1] is the center of the Gaussian,
;a_coeff[2] is the width (the standard deviation) of the Gaussian

;*****Uncomment this (or parts of it) to plot histograms****
;if frame eq 500 then begin
      ;     plot, x_gauss[0:200]*binsz+hmin, h
;     oplot,x_gauss[0:200]*binsz+hmin, g
;endif


end
```

Section A3: Baseline Fitting Routine

Routine: CH4_DATFIT.PRO
Purpose: Convert JD time to phase, fit a baseline to the data and subtract it.

```
;*****RESTORE THE VARIABLES*****

restore, 'idl_save/ch4_comflux.sav'

;*****SOME HOUSE KEEPING*****

f1sz = size(flux1, /dim)

;*****NORMALIZE THE FLUX TO 1******

flux1[*,0] = flux1[*,0]/(mean(flux1[*,0],/NAN))
;flux2[*,0] = flux2[*,0]/(mean(flux2[*,0],/NAN))
;we only work on star 1 (HAT-P-1b)

;*****JD-->HJD-->ECLIPSE PHASE*****

taxis  = helio_jd(flux1[*,1] + 54050.0d, ten(22,57,46.8)*15,
  ten(38,40,28.0))

phase = make_array(f1sz[0])
phase[*] = (taxis[*] - 53984.397d)/4.46529d
phase[*] = phase[*] - fix(phase[*])

;*****FIT A BASE LINE TO THE RAMP*****
;NOTE: We want to fit the baseline only in non-eclipse data points, so:

use = where((flux1[*,1] le 48.21)or(flux1[*,1] ge 48.34))
plot, phase[use], flux1[use,0], title = 'Channel 4, brightness vs time,$
  outside eclipse', psym = 6, yrange = [0.90,1.10]

rms_best = 1.0d+10
for itry = 0,1000 do begin
    del= 0.000000005*(double(itry))
    fit= make_array(f1sz)
    x1 = alog(phase+del-min(phase))
    x2 = phase+del
    x  = [transpose(x1[use]),transpose(x2[use])]
```

```
    res= regress(x,flux1[use,0],const=z)
    fit= (res[0]*x1 + res[1]*x2 + z)
    diffl= (flux1[use,0] - fit[use])/fit[use]
    rms = sqrt(mean(diffl^2))
    if rms lt rms_best then begin
        rms_best = rms
        ibest = itry
        base = make_array(f1sz[0])
        base = fit
    endif
endfor
ramparr=base


;*****SUBTRACT THE LINE FROM THE RAMPED RESULTS*****

flux1[*,0] = flux1[*,0]-ramparr[*] + 1
oneArr = make_array(size(ramparr, /dim))
oneArr[*] = 1   ;array that has all its elements = 1

;*****PLOT THE RESULTS*****
plot,phase, flux1[*,0]
oplot,phase, oneArr

;*****SAVE VARIABLES*****

save, filename='idl_save/ch4_datfit.sav'

end
```

Section A4: Eclipse Fitting Routine

Routine: CH4_ECLFIT.PRO
Purpose: Try 1 000 000 versions of the eclipse model, and calculate their chi-squared
   values.
   Fit the best model to the data again, so we can plot it to the screen

```
;*****RESTORE THE VARIABLES*****

restore, 'idl_save/ch4_datfit.sav'

;*****TEST MANY SECONDARY ECLIPSE MODEL CURVES****

chi_best = 9999999.
i_best = -1.0
j_best = -1.0
k_best = -1.0
start_l  = 0.009
start_w  = 0.004
start_ph = 0.485
for i = 0,100 do begin
    for j = 0,100 do begin
        for k = 0,100 do begin
            model  = ch4_model(f1sz[0],start_w+0.00004*i ,
  start_l+0.00011*j,$
```

```
                              start_ph+0.00005*k, phase)
          mphi   = [0.2, 0.3, 0.4, phi,   0.6, 0.7, 0.8]
          minten = [1.0, 1.0, 1.0, model, 1.0, 1.0, 1.0]
          yinten = model

          ;*****FIT THE ECLIPSE CURVE TO THE DATA*****

          edepth  = linfit(yinten, flux1[*,0])
          fitbest = edepth[0]+ edepth[1]*yinten[*]
          diff = flux1[*,0] - fitbest
          scat = stddev(diff)
          scatvec    = make_array(f1sz[0])
          scatvec[*] = scat
          edepth =linfit(yinten, flux1[*,0], measure_errors=scatvec,$
                                                  sigma=sigma)
          fitbest= edepth[0] + edepth[1]*yinten[*]
          chisqr =total((diff(*)/scatvec(*))^2)
          if chisqr lt chi_best then begin
             chi_best = chisqr
             i_best = i
             j_best = j
             k_best = k
          endif
       endfor
    endfor
endfor
;*****FIT BEST MODEL TO DATA*****

model  = ch4_model(f1sz[0],start_w+0.00004*i_best ,
  start_l+0.00011*j_best,$ start_ph+0.00005*k_best, phase)
mphi   = [0.2, 0.3, 0.4, phi,   0.6, 0.7, 0.8]
minten = [1.0, 1.0, 1.0, model, 1.0, 1.0, 1.0]
yinten = model
edepth  = linfit(yinten, flux1[*,0])
fitbest = edepth[0]+ edepth[1]*yinten[*]
diff = flux1[*,0] - fitbest
scat = stddev(diff)
scatvec    = make_array(f1sz[0])
scatvec[*] = scat
edepth = linfit(yinten, flux1[*,0], measure_errors=scatvec, sigma=sigma)
fitbest= edepth[0] + edepth[1]*yinten[*]
print, 'depth of the eclipse is: ',edepth[1]
;*****PLOT THE RESULTS*****
plot,phase,flux1[*,0]
oplot, phase, fitbest
save, filename='ch4_fitted_eclipse.sav'

end
```

Section A5: Model Creation Function

Function: CH4_MODEL.PRO
Note: Called from within CH4_ECLFIT.PRO (see A4)
Purpose: Create a model curve point for parameters given so that the eclipse depth can be
   determined by the calling routine.

```
function ch4_model, msz, w, l, x1, phase

;*****THIS FUNCTION MAKES AN ECLIPSE MODEL FOR TRANSITING EXOPLENTS
;INPUT VARIABLES:
;W = THE WIDTH OF THE PART WHERE BRIGHTNESS IS ACTUALLY
;    CHANGING-DECREASING AT FIRST AND LATER INCREASING BACK TO NORMAL
;L = THE LENGTH OF THE FLAT BOTTOM PART
;X1= THE STARTING POINT (IN PHASE UNITS) OF THE ECLIPSE, WHEN THE
;    LIGHT FIRST STARTS TO DECREASE.
;MSZ= THE SIZE OF THE MODEL ARRAY NEEDED

model    = make_array(msz)
model[*] = 1.0

model[where(phase[*] gt (x1+w)and(phase[*] lt (x1+w+l)))] = 0

f1 = (-1/w)*phase[*] + (1/w)*(x1+w);f1 is the first slope of the transit
                                   ;when the brightness is decreasing
model[where(phase[*]gt(x1)and(phase[*]lt(x1+w)))]=f1[where(phase[*] gt $
                                         (x1)and(phase[*] lt (x1+w)))]

f2 = (1/w)*phase[*]-(1/w)*(x1+w+l);f2 is the second slope of the transit
                                  ;when the brightness is increasing
model[where(phase[*] gt (x1+w+l)and $
         (phase[*] lt (x1+2*w+l)))]$
  =f2[where(phase[*] gt (x1+w+l)and $
         (phase[*] lt (x1+2*w+l)))]

return, model[*]

end
```

Section A6: Random Error Estimation Routine

Routine: CH4_MONTE_CARLO.PRO
Purpose: Bootstrap Monte Carlo estimation of random error on the eclipse depth.

```
;*****RESTORE THE VARIABLES*****

restore, 'ch4_fitted_eclipse.sav'

;*****MAKE FAKE DATA*****

nfds  = 1000            ;number of fake data sets

errarr= make_array(nfds, 4);errarr will hold: depth of the fake
                           ;data set, wings width
                           ;(w),full eclipse length(l)
                           ;and starting phase of the
                           ;eclipse (ph)

devs = flux1[*,0]-fitbest  ;deviations of real data from best fit model
```

```
;*****BIG LOOP****

for n = 0,nfds-1 do begin
    fdata= devs[scramble(f1sz[0])]+fitbest ;fake data array.
                                           ;We have just randomized the
                                           ;deviations of the real data
                                           ;from the best fit and added
                                           ;them to it.

    ;*****TEST MANY SECONDARY ECLIPSE MODEL CURVES****

    chi_best_f = 9999999.   ;the _f stands for fake, since
                            ;this is a "fake data" operation
    i_best_f   = -1.0
    j_best_f   = -1.0
    k_best_f   = -1.0
    start_l_f  = 0.009
    start_w_f  = 0.004
    start_ph_f = 0.485
    for fi = 0,100 do begin         ;fi, fj and fk = fake i, j and k
                                    ;from identical indices in
  ch4_eclfit.pro
        for fj = 0,100 do begin
            for fk = 0,100 do begin
                model   = ch4_model(f1sz[0],start_w_f+0.00004*fi ,
  start_l_f+0.00011*fj, start_ph_f+0.00005*fk, phase)
                mphi    = [0.2, 0.3, 0.4, phi,   0.6, 0.7, 0.8]
                minten  = [1.0, 1.0, 1.0, model, 1.0, 1.0, 1.0]
                yinten  = model

                ;*****FIT THE ECLIPSE CURVE TO THE DATA*****
                edepth_f  = linfit(yinten, fdata)
                fitbest_f = edepth[0]+ edepth[1]*yinten[*]
                diff_f    = fdata - fitbest_f
                scat_f    = stddev(diff_f)
                scatvec_f = make_array(f1sz[0])
                scatvec_f[*]= scat_f
                edepth_f = linfit(yinten,fdata,measure_errors=scatvec_f,$
                                                    sigma=sigma_f)
                fitbest_f= edepth_f[0] + edepth_f[1]*yinten[*]
                chisqr_f = total((diff_f[*]/scatvec_f[*])^2)
                if chisqr_f lt chi_best_f then begin
                    chi_best_f = chisqr_f
                    i_best_f = fi
                    j_best_f = fj
                    k_best_f = fk
                endif
            endfor
        endfor
    endfor

    ;*****FIT BEST MODEL TO DATA*****
    model  = ch4_model(f1sz[0],start_w_f+0.00004*i_best_f,$
                    start_l_f+0.00011*j_best_f, $
                    start_ph_f+0.00005*k_best_f, phase)
    mphi   = [0.2, 0.3, 0.4, phi,   0.6, 0.7, 0.8]
    minten = [1.0, 1.0, 1.0, model, 1.0, 1.0, 1.0]
```

```
    yinten = model
    edepth_f  = linfit(yinten, fdata)
    fitbest_f = edepth_f[0]+ edepth_f[1]*yinten[*]
    diff_f    = fdata - fitbest_f
    scat_f    = stddev(diff_f)
    scatvec_f    = make_array(f1sz[0])
    scatvec_f[*] = scat_f
    edepth_f     = linfit(yinten, fdata, MEASURE_ERRORS=scatvec_f,$
                                         sigma=sigma_f)
    fitbest_f    = edepth_f[0] + edepth_f[1]*yinten[*]
    errarr[n,*]=[edepth_f[1],start_w_f+0.00004*i_best_f ,$
                             start_l_f+0.00011*j_best_f, $
                             start_ph_f+0.00005*k_best_f]
endfor  ;END BIG LOOP

save, filename='ch4_monte_carlo_fits.sav'

end
```

Section A7: Binned Plots Routine

Routine: CH4_ECLBIN.PRO
Purpose: Bin the data, so that it can be plotted without cluttering the plot.
   Make the eclipse easily visible.

```
binsz = 20

restore, 'ch4_fitted_eclipse.sav'
;variables used from the 'restore':
;     yinten - values for the model eclipse
;     fitbest- best fit eclipse curve
;     f1sz   - dimensions of the phot data array
;     flux1  - phot data and phase array
;     phase  - phase array

;***** MAKE THE ARRAYS TO HOLD THE BINS *****
if (f1sz[0] mod binsz) eq 0 then begin
    mbr = make_array(f1sz[0]/binsz)
    mph = make_array(f1sz[0]/binsz)
endif else begin
    mbr = make_array(f1sz[0]/binsz+1)
    mph = make_array(f1sz[0]/binsz+1)
endelse

;***** ACTUAL BINNING *****
i = 0
while i+binsz lt f1sz[0] do begin
    mbr    [i/binsz] = mean(flux1  [i:i+binsz,0])
    mph    [i/binsz] = mean(phase  [i:i+binsz ])
    yinten [i/binsz] = mean(yinten [i:i+binsz ])
    fitbest[i/binsz] = mean(fitbest[i:i+binsz ])
    i = i+binsz
```

```
endwhile

if (f1sz[0] mod binsz) ne 0 then begin
 mbr[f1sz[0]/binsz]=mean(flux1[f1sz[0]-(f1sz[0]mod binsz):f1sz[0]-1,0])
 mph[f1sz[0]/binsz]=mean(phase[f1sz[0]-(f1sz[0]mod binsz):f1sz[0]-1  ])
 yinten[f1sz[0]/binsz]=mean(yinten[f1sz[0]-(f1sz[0]mod binsz):f1sz[0]-1])
 fitbest[f1sz[0]/binsz]=mean(fitbes[f1sz[0]-(f1sz[0]mod binsz):f1sz[0]-1 ])
endif

;the values 0.0020 and 0.0014 are chosen, because at the time I added
;these lines, I already knew the errors from the Monte Carlo simulations
fitmaxb = 1.0-0.0020 + 0.0020*yinten[*]
fitminb = 1.0-0.0014 + 0.0014*yinten[*]

;***** plot the results *****
plot, mph, mbr, yrange=[0.99, 1.01]

end
```

Section A8: Routines used which are not included in the Standard IDL Library

readfits - Source: readfits.pro. Reads FITS image files to IDL 2-dimensional arrays. Part of the IDL Astronomy User's Library, available at *http://idlastro.gsfc.nasa.gov/contents.html*

juldate – Source: juldate.pro. Converts calendar date to Reduced Julian Date. Part of the IDL Astronomy User's Library, available at *http://idlastro.gsfc.nasa.gov/contents.html*

helio_jd – Source: helio_jd.pro. Converts geocentric Reduced Julian Date to Heliocentric Julian Date. Part of the IDL Astronomy User's Library, available at *http://idlastro.gsfc.nasa.gov/contents.html*

ten – Source: ten.pro. Converts sexigesimal numbers to decimal e.g. "hour or degree":min:sec to decimal hours or degrees. Part of the IDL Astronomy User's Library, available at *http://idlastro.gsfc.nasa.gov/contents.html*

scramble – Source: scramble.pro is written by R. Sterner. It scrambles randomly the entries of an array. Available at *http://132.248.1.102/~morisset/idl/pro/juhapl/pro/scramble.pro*

References

Bakos, G. A., R. W. Noyes, G. Kovacs, D. W. Latham, D. D. Sasselov, G. Torres, D. A. Fischer, et al. 2007. HAT-P-1b: A large-radius, low-density exoplanet transiting one member of a stellar binary. *Astrophysical Journal* **656**, 552-559.

Beaulieu, J. P., D. P. Bennett, P. Fouque, A. Williams, M. Dominik, U. G. Jorgensen, D. Kubas, et al. 2006. Discovery of a cool planet of 5.5 Earth masses through gravitational microlensing. *Nature* **439**, 437-440.

Böhm-Vitense, E. 1991. *Introduction to stellar astrophysics. vol. 1: Basic stellar observations and data*. 2nd ed. Vol. 1., 80-83 Great Britain: Cambridge University Press.

Bond, I. A., A. Udalski, M. Jaroszynski, N. J. Rattenbury, B. Paczynski, I. Soszynski, L. Wyrzykowski, et al. 2004. Ogle 2003-blg-235. *Astrophysical Journal* **606**, L155-L158.

Brown, T. M., D. Charbonneau, R. L. Gilliland, R. W. Noyes, and A. Burrows. 2001. Hubble space telescope time-series photometry of the transiting planet of HD 209458. *Astrophysical Journal* **552**, 699.

Burgdorf, M. J., D. M. Bramich, M. Dominik, M. F. Bode, K. D. Horne, I. A. Steele, N. Rattenbury, and Y. Tsapras. 2007. Exoplanet detection via microlensing with RoboNet-1.0. *Planetary and Space Science* **55**, 582-588.

Butler, R. P., J. T. Wright, G. W. Marcy, D. A. Fischer, S. S. Vogt, C. G. Tinney, H. R. A. Jones, et al. 2006. Catalog of nearby exoplanets. *Astrophysical Journal* **646**, 505-522.

Carroll, B. W., and D. A. Ostlie. 1996. *An introduction to modern astrophysics*. 1st ed., 46, USA: Addison-Wesley Pub.

Charbonneau, D., L. E. Allen, S. T. Megeath, G. Torres, R. Alonso, T. M. Brown, R. L. Gilliland, et al. 2005. Detection of thermal emission from an extrasolar planet. *Astrophysical Journal* **626**, 523-529.

Charbonneau, D., T. M. Brown, R. W. Noyes, and R. L. Gilliland. 2002. Detection of an extrasolar planet atmosphere. *Astrophysical Journal* **568**, 377-384.

Chauvin, G., A. M. Lagrange, C. Dumas, B. Zuckerman, D. Mouillet, I. Song, J. L. Beuzit, and P. Lowrance. 2005. Giant planet companion to 2MASSW J1207334-393254. *Astronomy and Astrophysics* **438**, L25-L28.

———. 2004. A giant planet candidate near a young brown dwarf - direct VLT/NACO observations using IR wavefront sensing. *Astronomy & Astrophysics* **425**, L29-32.

Deming, D. 2007. Private communication.

Deming, D., S. Seager, L. J. Richardson, and J. Harrington. 2005. Infrared radiation from an extrasolar planet. *Nature* **434**, 740-743.

Fazio, G. G., J. L. Hora, L. E. Allen, M. L. N. Ashby, P. Barmby, L. K. Deutsch, J. -S Huang, et al. 2004. The infrared array camera (IRAC) for the spitzer space telescope. *The Astrophysical Journal Supplement Series* **154**, 10-17.

Gould, A., A. Udalski, D. An, D. P. Bennett, A. Y. Zhou, S. Dong, N. J. Rattenbury, et al. 2006. Microlens OGLE-2005-BLG-169 implies that cool neptune-like planets are common. *Astrophysical Journal* **644**, L37-40.

Knutson, Heather A., David Charbonneau, Lori E. Allen, Adam Burrows, and S. Thomas Megeath. 2008. The 3.6–8.0 μm broadband emission spectrum of HD 209458b: Evidence for an atmospheric temperature inversion. *The Astrophysical Journal* **673**, 526-531.

Mayor, Michel, and Didier Queloz. 1995. A Jupiter-mass companion to a solar-type star. *Nature* **378**, 355.

PLANET Collaboration. The search for extra-solar planets by microlensing. 2007[cited 12/05 2007]. Available from http://planet.iap.fr/planeet.html.

Press, W. H., S. A. Teukolsky, W. T. Vetterling, and B. P. Flannery. 1992. *Numerical recipes in C*. 2nd ed. USA: Press Syndicate of the University of Cambridge.

Schneider, J. The extrasolar planet encyclopaedia, interactive extrasolar planet catalog. 2008 [cited 03/21 2008]. Available from http://exoplanet.eu/catalog.php.

———. The extrasolar planets encyclopedia, interacive extra-solar planets catalog - 1.a. candidates detected by transit. 2007 [cited 12/05 2007]. Available from http://exoplanet.eu/catalog-transit.php.

———. The extrasolar planets encyclopedia, interactive extra-solar planets catalog - 1.b. candidates detected by microlensing. 2006 [cited 12/05 2007]. Available from http://exoplanet.eu/catalog-microlensing.php.

Spitzer Science Center. IRAC: Instrument description. 2006 [cited 03/09 2008]. Available from http://ssc.spitzer.caltech.edu/irac/descrip.html.

Swain, M. R., G. Vasisht, and G. Tinetti. 2008. The presence os methane in the atmosphere of an extrasolar planet. *Nature* **452**, 329.

Taylor, J. R. 1997. 12.2 General definition of chi squared. In *An introduction to error analysis*, ed. A. McGuire. 2nd ed., 265. USA: University Science Books.

Udry, S., X. Bonfils, X. Delfosse, T. Forveille, M. Mayor, C. Perrier, F. Bouchy, et al. 2007. The HARPS search for southern extra-solar planets   - XI. Super-Earths (5 and 8 *M*) in a 3-planet system. *Astronomy and Astrophysics* **469**, L43-L47.

Van de Kamp, P. 1963. Astrometric study of Barnard's star from plates taken with the 24-inch Sproul refractor. *Astrophysical Journal* **68**, 515.

Wolszczan, Alexander. 1994. Confirmation of Earth-mass planets orbiting the millisecond pulsar PSR B1257+12. *Science* **264**, 538.

Zeilik, M., and S. A. Gregory. 1998. *Introductory astronomy and astrophysics*, eds. J. Vondeling, J. Bortel and L. Boyle. 4th ed. USA: Thomson Learning, Inc. Thomson Learning.